



## ISTITUTO NAZIONALE DI RICERCA METROLOGICA Repository Istituzionale

Skin effect in steel sheets under rotating induction

This is the author's accepted version of the contribution published as:

*Original*

Skin effect in steel sheets under rotating induction / Appino, Carlo; O., Hamrit; F., Fiorillo; C., Ragusa; O., de la Barrière; F., Mazaleyrat; M., Lobue. - In: INTERNATIONAL JOURNAL OF APPLIED ELECTROMAGNETICS AND MECHANICS. - ISSN 1383-5416. - 48:(2015), pp. 247-254.

*Availability:*

This version is available at: 11696/31355 since: 2021-02-07T07:47:26Z

*Publisher:*

IOS

*Published*

DOI:

*Terms of use:*

This article is made available under terms and conditions as specified in the corresponding bibliographic description in the repository

*Publisher copyright*

(Article begins on next page)

# Skin effect in steel sheets under rotating induction

C. Appino<sup>1</sup>, O. Hamrit<sup>2</sup>, F. Fiorillo<sup>1</sup>, C. Ragusa<sup>3</sup>, O. de la Barrière<sup>2a</sup>, F. Mazaleyrat<sup>2</sup>, M. LoBue<sup>2</sup>

<sup>1</sup>Istituto Nazionale di Ricerca Metrologica (INRIM), Strada delle cacce 91, 10135 Torino, Italy

<sup>2</sup>SATIE, ENS Cachan, CNRS, UniverSud, 61 av. du Président Wilson, F-94230 Cachan, France

<sup>3</sup>Dipartimento Energia, Politecnico di Torino, C.so Duca degli Abruzzi 24, 10129 Torino, Italy

---

<sup>a</sup> Corresponding author. Electronic address: [barriere@satie.ens-cachan.fr](mailto:barriere@satie.ens-cachan.fr), telephone: 0033147402125.

## Abstract

By means of a newly developed broadband measuring setup we have overcome the usual upper limit for the test frequency, around a few hundred Hz, which is encountered in the two-dimensional characterization of magnetic steel sheets at technical inductions and we have measured the rotational losses in low-carbon steels up to 1 kHz and peak induction 1.7 T. An important piece of information is thus retrieved upon a frequency range useful to predict the performance of high-speed electrical machines. Our experiments, performed on thick (0.640 mm) laminations, have brought to light the emergence of the skin effect under rotational fields. This is revealed by an abrupt deviation of the excess loss component, calculated under the conventional loss separation procedure, from its well-known linear dependence on the square root of the frequency. A simple magnetic constitutive law under rotating induction is proposed and introduced into the electromagnetic diffusion equation, which is solved by finite elements coupled to a non-linear algorithm. The classical rotational eddy current loss, largely prevalent with respect to the hysteresis and excess loss components on approaching the kHz frequencies in low-carbon steels, is then calculated in the presence of skin effect, permitting one to achieve full analysis of the rotational losses and good predicting capability upon a broad range of frequencies and peak inductions.

## 16 1- Introduction

17 In electrical traction applications, compact geometry and maximum torque density of motors are obtained by  
18 increasing the rotating speed [1, 2], with ensuing high conversion frequencies, greater iron losses, and decreasing  
19 efficiency. A compromise must then be found at the design stage between these competing issues, a reason for  
20 requiring accurate broadband magnetic loss characterization of the laminations used in the machine cores and a  
21 relatively simple implementation of loss modeling. The loss decomposition procedure, including the case of  
22 distorted induction, is the standard modeling response to the loss phenomenology at low-to-medium frequencies,  
23 where the skin effect can be neglected [3, 4]. Starting from solid physical analysis, it provides a simple three-  
24 term expression for the measured energy loss  $W(f) = W_{\text{hyst}} + W_{\text{class}}(f) + W_{\text{exc}}(f)$ , where the quasi-static term  $W_{\text{hyst}}$   
25 combines with a dynamic contribution  $W_{\text{dyn}}(f) = W_{\text{class}}(f) + W_{\text{exc}}(f)$ , the sum of the classical and the excess  
26 components, which depend on the magnetizing frequency like  $f$  and  $f^{1/2}$ , respectively [3]. When, under  
27 increasing  $f$ , eddy current shielding gives rise to skin depth comparable to or lower than the lamination half-  
28 thickness, straightforward loss separation cannot be accomplished and the calculation of the dynamic loss  
29 component via the electromagnetic diffusion equation requires modeling (for example, via the Preisach model of  
30 hysteresis) of the constitutive equation of the material and the use of numerical methods [5-8].

31 It has been shown that conventional loss separation can be applied, in the absence of skin effect, to the two-  
32 dimensional losses, and one can express, in particular, the rotational losses as  $W^{(\text{ROT})}(f) = W_{\text{hyst}}^{(\text{ROT})} + W_{\text{class}}^{(\text{ROT})}(f)$   
33  $+ W_{\text{exc}}^{(\text{ROT})}(f)$ , with the same  $W_{\text{class}}^{(\text{ROT})} \propto f$  and  $W_{\text{exc}}^{(\text{ROT})} \propto f^{1/2}$  dependences found under alternating fields [9]. Very  
34 little is known, however, on the behavior of the rotational losses beyond a few hundred Hz [10], that is, under the  
35 regimes pertaining to high-speed electrical machines, where skin effect will expectedly take place.

36 We have employed a recently developed 2D setup, based on a three-phase magnetizer [11], to attain  
37 rotational induction levels of technical interest (e.g.  $J_p = 1.5$  T and beyond) in non-oriented steel sheets up to the  
38 kHz range [12]. We have investigated, in particular, the rotational loss behavior versus frequency of low-carbon  
39 steel sheets, 0.640 mm thick, up to 1 kHz and peak polarization  $J_p = 1.7$  T. Conductivity and thickness of these  
40 sheets are sufficient to generate a surge of the skin effect already at power frequencies. A sort of frequency  
41 threshold for it is in fact identified, where an attendant sharp deviation of  $W_{\text{exc}}^{(\text{ROT})}$  from the usual  $f^{1/2}$  dependence  
42 is put in evidence when applying the standard loss decomposition procedure. This appears to be a unique simple  
43 experimental route to direct recognition of growing skin effect. It also highlights the conceptually important role  
44 of the excess component in the loss analysis, even if, as in the present case, it marginal contributes to the total  
45 loss figure. To calculate the classical loss, by far the largest component in the upper frequency range, it is  
46 recognized that, thanks to the near-isotropic properties of the material, the magnetic constitutive law  $B(H)$  under  
47 rotational field can be well approximated, along any of two orthogonal directions, by a simple relationship  
48 between complex quantities of the type  $\underline{B} = \underline{\mu}(\underline{H}) \cdot \underline{H}$ . This permits one to solve the electromagnetic diffusion  
49 equation by conventional numerical technique and to calculate  $W_{\text{class}}^{(\text{ROT})}(f)$ , eventually attaining good prediction  
50 of  $W^{(\text{ROT})}(f)$  upon the whole investigated frequency range.

51

## 52 2. Experimental results: evidence for the skin effect

53 A three-phase magnetizer, especially designed to reach high frequencies [11], has been employed in the  
 54 measurement of the magnetic losses in low-carbon steel sheets (density  $\delta = 7850 \text{ kg/m}^3$ , thickness  $d = 0.640 \text{ mm}$ ,  
 55 resistivity  $\rho = 12.51 \cdot 10^{-8} \text{ } \Omega \cdot \text{m}$ ) under digitally controlled circular flux loci [13]. The magnetic losses have been  
 56 measured by the fieldmetric method [14-15] on 80 mm diameter circular samples, accurately centred in the  
 57 stator-like magnetizer. A small air-gap of 1 mm permits one to minimize the required exciting power, which is  
 58 supplied by triple DC-20 kHz 5 kVA power amplifier (CROWN 5000VZ). The orthogonal  $B$  and  $H$  windings are  
 59 placed on a 20 mm  $\times$  20 mm measuring area at the centre of the disk. The measurements are repeated, for any  
 60 polarization and frequency value, under clockwise and counterclockwise rotation and their average is taken as  
 61 the resulting loss figure  $W^{(\text{ROT})}(J_p, f)$ . Fig. 1 shows the experimental dependence of the measured rotational loss  
 62 on  $J_p$  (negligibly different everywhere from the peak induction  $B_p$ ) up to 1.7 T for frequencies ranging between 2  
 63 Hz and 1kHz. It is noted how the maximum of  $W^{(\text{ROT})}(f)$  versus  $J_p$ , occurring around  $J_p = 1.5 \text{ T}$ , tends to  
 64 disappear beyond about 50 Hz, because of the growing influence of the monotonically increasing classical loss  
 65 component. It is also remarked that the upper values of the here attained product  $J_p \cdot f$  (e.g.,  $J_p = 1.5 \text{ T}$  at  $f = 1$   
 66 kHz) are significantly larger than present literature limits [10].

67 According to the standard analysis performed at power frequencies in nonoriented Fe-Si laminations [9], the  
 68 rotational hysteresis  $W_{\text{hyst}}^{(\text{ROT})}$  is found by extrapolating  $W^{(\text{ROT})}(J_p, f)$  to  $f = 0$  and we calculate the classical loss  
 69  $W_{\text{class}}^{(\text{ROT})}(f)$  as

$$70 \quad W_{\text{class}}^{(\text{ROT})}(B_p, f) = \frac{\pi^2}{3} \cdot \frac{d^2 B_p^2}{\rho} f. \quad [\text{J/m}^3] \quad (1)$$

71 By making the difference  $W_{\text{diff}}^{(\text{ROT})}(f) = W^{(\text{ROT})}(f) - W_{\text{class}}^{(\text{ROT})}(f) = W_{\text{hyst}}^{(\text{ROT})} + W_{\text{exc}}^{(\text{ROT})}(f)$ , we obtain the behaviors  
 72 shown in Fig. 2a (symbols), where the quantity  $W_{\text{diff}}^{(\text{ROT})}(f)$  is plotted against  $f^{1/2}$  for three different induction  
 73 levels.  $W_{\text{diff}}^{(\text{ROT})}(f)$  strongly deviates, beyond a threshold frequency value  $f_{\text{thr}}$ , from the usual  $f^{1/2}$  dependence (the  
 74 straight lines in Fig. 2a) experimentally observed below and around power frequencies in 3 wt% Fe-Si  
 75 laminations [16].  $W_{\text{diff}}^{(\text{ROT})}(f)$  follows opposite outward trends with respect to the  $f^{1/2}$  straight line below and above  
 76  $J_p \sim 1 \text{ T}$ , because  $W_{\text{class}}^{(\text{ROT})}(f)$  tends either to lower or faster than linear dependence on  $f$  and Eq. (1) no more  
 77 applies. Such behavior of  $W_{\text{class}}^{(\text{ROT})}(f)$  replicates the phenomenology of the alternating classical loss in the  
 78 presence of the skin effect [3-5] and is further put in evidence by the statistical analysis of the magnetic objects  
 79 (MO), as defined in Bertotti's theory [3]. Fig. 2 shows the dramatic departure of the number  $n(H_{\text{exc}})$  of active  
 80 MOs from the linear increase with  $H_{\text{exc}} = W_{\text{exc}}^{(\text{ROT})}/4J_p$  predicted using Eq. (1). The sharp turnaround of  $n(H_{\text{exc}})$   
 81 occurs exactly at the frequency  $f_{\text{thr}}$ . The statistical loss analysis provides then us with a direct and unique method  
 82 to detect the surge of the skin effect in magnetic sheets, even though, like in the present case,  $W_{\text{exc}}^{(\text{ROT})}$   
 83 contributes by a small proportion to  $W^{(\text{ROT})}$ . We have for example, at  $J_p = 1.2 \text{ T}$  and  $f_{\text{thr}} = 100 \text{ Hz}$ , the total  
 84 rotational loss  $W^{(\text{ROT})} = 360.5 \text{ mJ/kg}$ , composed of  $W_{\text{hyst}}^{(\text{ROT})} = 139.5 \text{ mJ/kg}$ ,  $W_{\text{class}}^{(\text{ROT})} = 197.5 \text{ mJ/kg}$ , and  $W_{\text{exc}}^{(\text{ROT})}$   
 85  $= 23.5 \text{ mJ/kg}$ . It is remarked that, given the mechanism of the magnetization rotation in nonoriented materials,  
 86 there is no room for classical loss formulations deriving from the saturation wave model, as sometimes proposed

87 in the literature [17].

88 Having thus experimentally identified a threshold frequency for the skin effect, we essentially need to  
89 proceed towards a novel formulation for  $W_{\text{class}}^{(\text{ROT})}(f)$ , by which we can cover the rotational loss properties upon  
90 the whole broad frequency range.

### 92 **3. Skin effect and classical eddy current losses under circular induction**

#### 93 *3.1 A simplified constitutive equation*

94 Let us take the sheet sample midplane as the  $xy$ -plane and assume the coordinate  $z = 0$  at the center of the  
95 disk sample. The magnetization vector is assumed to rotate at constant angular velocity  $\omega = 2\pi f$ . We need to  
96 define a constitutive equation for the material under rotating field, paralleling the usual case of alternating field,  
97 where such equation coincides with the static hysteresis loop and a hysteresis model must be worked out [4, 18].  
98 Remarkably, a simple magnetic constitutive law can be adopted with circular polarization in nonoriented alloys,  
99 under the following assumptions: 1) The constitutive relationship is rate independent. This amounts to assume,  
100 according to the experiments, that in the range of frequencies of interest (i.e., beyond  $f_{\text{thr}}$ ) the excess loss figure  
101  $W_{\text{exc}}^{(\text{ROT})}$  is much smaller than  $W_{\text{hyst}}^{(\text{ROT})}$  and  $W_{\text{class}}^{(\text{ROT})}$ ; 2) The material anisotropy can be neglected. We  
102 approximate here this condition by substituting, at each frequency, the experimental magnetic field locus  $\mathbf{H}(f)$   
103 associated with the circular  $\mathbf{B}$ -locus (of modulus  $B_p = |\mathbf{B}|$ ) with an equivalent circular  $\mathbf{H}$ -locus of same area and  
104 radius  $H(f) = |\mathbf{H}(f)|$ , emulating the condition of a perfectly isotropic material. By extrapolating this procedure to  $f$   
105  $= 0$ , the limiting circle of radius  $H_0 = |\mathbf{H}_0|$  is obtained, with  $\mathbf{B}$  lagging behind  $\mathbf{H}_0$  by the angle  $\theta_{\text{hyst}}$ . Under the  
106 isotropic approximation, the sinusoidal  $\mathbf{H}$  and  $\mathbf{B}$  components are identical along the  $x$  and  $y$  axes and the energy  
107 loss

$$108 \quad W^{(\text{ROT})}(B_p, f) = \oint \mathbf{H} \cdot d\mathbf{B} = \int_0^{1/f} (H_x \cdot dB_x / dt + H_y \cdot dB_y / dt) = W_x + W_y = 2W_x, \quad [\text{J/m}^3] \quad (2)$$

109 can be written in the quasi-static limit as  $W_{\text{hyst}}^{(\text{ROT})} = 2\pi H_0 B_p \omega \sin(\theta_{\text{hyst}})$ . The phase shift is then obtained as

$$110 \quad \theta_{\text{hyst}}(H_0) = \arcsin \left[ \frac{W_{\text{hyst}}^{(\text{ROT})}(B_p)}{2\pi H_0 B_p} \right]. \quad (3)$$

111 At the same time, the complex permeability, embodying the constitutive equation for the material under  
112 rotational field, is given by

$$113 \quad \underline{\mu}(H_0) = \mu(H_0) \exp[-i\theta_{\text{hyst}}(H_0)] \quad (4)$$

114 (with  $i^2 = -1$ ), where  $\mu(H_0) = B_p/H_0$ . Both  $\underline{\mu}(H_0)$  and  $\theta_{\text{hyst}}$  are time-independent and evolve with the polarization  
115 level in the investigated material as shown in Fig. 4. The complex constitutive equations for the  $x$  and  $y$   
116 directions can thus be expressed as  $\underline{B}_x = \underline{\mu}(H_x)\underline{H}_x$  and  $\underline{B}_y = \underline{\mu}(H_y)\underline{H}_y$ , with  $H_x = |\underline{H}_x|$  and  $H_y = |\underline{H}_y|$ .

#### 117 *3.2 Diffusion equation and classical loss*

118 The electromagnetic diffusion equation, controlling the magnetic field penetration in the sheet, is written,  
119 under the usual assumption of infinitely extended  $xy$ -plane,

$$120 \quad \frac{\partial^2 \underline{H}_x(z)}{\partial z^2} = i\omega\sigma \underline{B}_x(z) \quad \frac{\partial^2 \underline{H}_y(z)}{\partial z^2} = i\omega\sigma \underline{B}_y(z) \quad (5)$$

121 where all the local quantities depend only on  $z$ . Introducing the constitutive equations in Eq. (5) we get

$$122 \quad \frac{\partial^2 \underline{H}_x(z)}{\partial z^2} = i\omega\sigma \underline{\mu}(H_x) \underline{H}_x \quad \frac{\partial^2 \underline{H}_y(z)}{\partial z^2} = i\omega\sigma \underline{\mu}(H_y) \underline{H}_y, \quad (6)$$

123 to be solved under the boundary conditions

$$124 \quad \left. \frac{\partial \underline{H}_x(z)}{\partial z} \right|_{z=0} = 0 \quad \left. \frac{\partial \underline{H}_y(z)}{\partial z} \right|_{z=0} = 0 \quad (7)$$

125

$$126 \quad \left. \frac{\partial \underline{H}_x(z)}{\partial z} \right|_{z=d/2} = i\omega\sigma \frac{d}{2} B_p \quad \left. \frac{\partial \underline{H}_y(z)}{\partial z} \right|_{z=d/2} = i\omega\sigma \frac{d}{2} B_p, \quad (8)$$

127 imposed by the symmetry of the magnetic field profile with respect to the  $z=0$  plane (Neumann condition) and  
 128 the requirement of a mean circular induction  $B_p$  across the sample thickness, respectively. This problem is non  
 129 linear, because  $\underline{\mu}$  depends on  $|\underline{H}|$ . We thus discretize Eq. (5) versus  $z$  by the Finite Elements Method and we  
 130 apply the Fixed Point (FP) iterative technique [5] to solve the non linearity. Its solution provides the  $\underline{H}(z)$  profile,  
 131 by which we can compute, via the constitutive equation, the classical loss  $W_{\text{class}}^{(\text{ROT}, \text{FP})}$  and obtain the hysteresis  
 132 loss component  $W_{\text{hyst}}^{(\text{ROT})}$ . Since the induction profile through the sample cross-section evolves with  $f$ , the same  
 133 holds for  $W_{\text{hyst}}^{(\text{ROT})}$ , as shown in Fig. 5. This behavior replicates to some extent the skin effect related increase of  
 134 the hysteresis loss with  $f$  observed under alternating fields [5, 7], but for the decrease of  $W_{\text{hyst}}^{(\text{ROT})}$  at the highest  $J_p$   
 135 values. Such a decrease is consistent with the experimental dependence of  $W_{\text{hyst}}^{(\text{ROT})}$  on  $J_p$ . After having attained a  
 136 maximum value, it tends to zero on approaching the saturation, following the disappearance of the domain walls.  
 137 If we define the quantity  $W^{(\text{ROT}, \text{FP})} = W_{\text{hyst}}^{(\text{ROT})} + W_{\text{class}}^{(\text{ROT}, \text{FP})}$ , the sum of the so-calculated hysteresis and classical  
 138 losses, we find that it accounts for most of the measured loss  $W_{\text{exp}}^{(\text{ROT})}$  beyond  $f_{\text{thr}}$ , while the conventional loss  
 139 separation holds below this threshold. Comparison of  $W_{\text{exp}}^{(\text{ROT})}$  with  $W^{(\text{ROT}, \text{FP})}$  is provided in Fig. 6 at  $f = 1$  kHz  
 140 and  $f = 100$  Hz. In both cases the excess loss, though crucial to the identification of the threshold frequency  $f_{\text{thr}}$   
 141 via Eq. (1), turns out to be a few percent of the total loss only. It is observed how  $W_{\text{class}}^{(\text{ROT})}$ , calculated with Eq.  
 142 (1), overestimates the measured loss at  $f = 1$  kHz and low inductions, while falling short of  $W_{\text{class}}^{(\text{ROT}, \text{FP})}$  at high  
 143 inductions, consistent with the results reported in Fig. 2.

144 We might inquire about a possible approximate expression for the classical rotational loss with skin effect  
 145 where, as often done with the alternating regime [3, 19], a linear material is considered. With constant complex  
 146 permeability  $\underline{\mu}$ , uniform across the lamination depth and depending only on the mean value  $B_p$ , we obtain a linear  
 147 diffusion equation, which can be analytically solved. If the correspondingly calculated classical loss is  
 148  $W_{\text{class}}^{(\text{ROT}, \text{LIN})}$ , a ratio  $F_{\text{class}}^{(\text{LIN})} = W_{\text{class}}^{(\text{ROT}, \text{LIN})} / W_{\text{class}}^{(\text{ROT})}$  is obtained through the equation

149

150

$$F_{\text{class}}^{(\text{LIN})}(d/\delta) = 3 \frac{(\sinh a_+ / a_+ - \sinh a_- / a_-)}{\cosh a_+ - \cos a_-} \quad (9)$$

151

152

153

154

155

156

157

158

159

where  $\delta = 1/(\pi|\underline{\mu}|\sigma)^{1/2}$  is the skin depth and  $a_{\pm} = (1 \pm \delta) d/\delta$ , with  $\delta = \tan(0.5\delta \arg(\underline{\mu}))$ , is a dimensionless quantity. It is interesting to parallel the ratio  $F_{\text{class}}^{(\text{LIN})}$  with the one concerning the previous numerical solution for the classical loss  $F_{\text{class}}^{(\text{FP})} = W_{\text{class}}^{(\text{ROT,FP})}/W_{\text{class}}^{(\text{ROT})}$ . These ratios are shown as a function of  $d/\delta$ , with the frequency ranging between DC and 1 kHz, for different values of  $J_p$ . The linear model, always providing a ratio  $F_{\text{class}}^{(\text{LIN})} < 1$ , cannot account for the effect of saturation on the lamination edges, a feature that can properly dealt with only by  $W_{\text{class}}^{(\text{ROT,FP})}$ . Remarkably, at high inductions, where  $F_{\text{class}}^{(\text{FP})} \geq 1$  (but relatively close to 1, as shown in Fig. 7), assuming  $F_{\text{class}} = 1$  (i.e. neglecting the skin effect) provides a better approximation of the experiments than the linear model.

#### 159 **4. Conclusions**

160

161

162

163

164

165

166

167

168

169

170

Magnetic losses have been measured under circular induction in 0.640 mm tick low-carbon steel laminations up to frequencies of 1 kHz and peak polarization level  $J_p = 1.7$  T. Relevant skin effect takes place, depending on the  $J_p$  value, starting from a few ten Hz, as uniquely revealed by the loss decomposition procedure, performed according to the statistical theory of losses. It is demonstrated that the classical loss component, always dominant beyond the threshold frequency for the skin effect, can be accurately computed exploiting a simplified magnetic constitutive law of the material under rotational field. It is also shown that the extreme simplification of assuming a fully linear approximation for the diffusion equation can provide acceptable results only at low induction levels.



- 172 [1] K.M. Rahman and S.E. Sculz, Design of high-efficiency and high-torque-density switched reluctance motor  
173 for vehicle propulsion, *IEEE Trans. Ind. Appl.*, **38** (2002), 1500-1507.
- 174 [2] S. Niu, . Ho, W. Fu, and J. Zhu, Eddy current reduction in High-Speed Machines and Eddy Current Loss  
175 Analysis With Multislice Time-Stepping Finite-Element Method, *IEEE Trans. Magn.*, **48** (2012), 1007-  
176 1010.
- 177 [3] G. Bertotti, *Hysteresis in Magnetism*, Academic Press, New York, 1998, Chap. 12.
- 178 [4] E. Barbisio, F. Fiorillo, and C. Ragusa, Predicting Loss in Magnetic Steels Under Arbitrary Induction  
179 Waveform and With Minor Hysteresis Loops, *IEEE Trans. Magn.*, **40** (2004), 1810-1819.
- 180 [5] C. Appino, G. Bertotti, O. Bottauscio, F. Fiorillo, P. Tiberto, D. Binesti, J.P. Ducreux, M. Chiampi, and M.  
181 Repetto, Power losses in thick steel laminations with hysteresis, *J. Appl. Phys.* **79** (1996), 4575-4577.
- 182 [6] V. Basso, G. Bertotti, O. Bottauscio, F. Fiorillo, M. Pasquale, M. Chiampi, and M. Repetto, Power losses in  
183 magnetic laminations with hysteresis: finite element modeling and experimental validation, *J. Appl. Phys.*  
184 **81** (1997), 5606-5608.
- 185 [7] S. E. Zirka, Y.I. Moroz, P. Marketos, and A.J. Moses, Evolution of power loss components with induction  
186 level and frequency, *J. Magn. Magn. Mater.* **320** (2008), e1039-e1043.
- 187 [8] C. Beatrice, C. Appino, O. de la Barrière, F. Fiorillo, and C. Ragusa, Broadband magnetic losses in Fe-Si  
188 and Fe-Co laminations, *IEEE Trans. Magn.*, **50** (2014), 6300504.
- 189 [9] C. Appino, C. Ragusa, and F. Fiorillo, Can rotational magnetization be theoretically assessed?, *Int. J. Appl.*  
190 *Electromagn. Mech.*, **44** (2014), 355-370.
- 191 [10] Y. Li, J. G. Zhu, Q. Yang, Z. W. Lin, Y. Guo, and C. Zhang, Study on rotational hysteresis and core loss  
192 under three dimensional magnetization, *IEEE Trans. Magn.*, **47** (2011), 3520-3523.
- 193 [11] O. de la Barrière, C. Appino, F. Fiorillo, C. Ragusa, M. Lecrivain, L. Rocchino, H. Ben Ahmed, M. Gabsi,  
194 F. Mazaleyrat, and M. LoBue, Extended frequency analysis of magnetic losses under rotating induction in  
195 soft magnetic composites, *J. Appl. Phys.*, **111** (2012), 07E325.
- 196 [12] C. Appino, O. de la Barrière, C. Beatrice, F. Fiorillo, and C. Ragusa, Rotational magnetic losses in  
197 nonoriented Fe-Si and Fe-Co laminations up to the kilohertz range, *IEEE Trans. Magn.*, **50** (2014), to  
198 appear.
- 199 [13] C. Ragusa and F. Fiorillo, A three-phase single sheet tester with digital control of flux loci based on the  
200 contraction mapping principle, *J. Magn. Magn. Mater.*, vol. 304, no. 2 (2006), pp. e568-e570.
- 201 [14] Y. Guo, J. Zhu, J. Zhong, H. Lu, and J. Jin, Measurement and modeling of rotational core losses of soft  
202 magnetic materials used in electrical machines: a review, *IEEE Trans. Magn.*, **44** (2008), 279-291.
- 203 [15] E. Cardelli, A. Faba, and F. Tissi, *Int. J. Appl. Electromagn. Mech.*, **44** (2014), 331-338.
- 204 [16] C. Appino, F. Fiorillo, and C. Ragusa, One-dimensional/two-dimensional loss measurements up to high  
205 inductions, *J. Appl. Phys.* **105** (2009), 07E718.
- 206 [17] S. Steentjes, S.E. Zirka, Y.E. Moroz, E.Y. Moroz, and K. Hameyer, Dynamic magnetization model of  
207 nonoriented steel sheets, *IEEE Trans. Magn.*, **50** (2014), 7300204.
- 208 [18] S.E. Zirka, Y.I. Moroz, P. Marketos, and A.J. Moses, Viscosity-based magnetodynamic model of soft  
209 magnetic materials, *IEEE Trans. Magn.*, **42** (2006), 2121-2132.
- 210 [19] I.D. Mayergoyz, F.M. Abdel-Kader, F.P. Emad, On penetration of electromagnetic fields into nonlinear  
211 conducting ferromagnetic media, *J. Appl. Phys.*, **55** (1984), 618-628.
- 212

213  
 214  
 215  
 216  
 217  
 218  
 219  
 220  
 221  
 222  
 223  
 224  
 225  
 226  
 227  
 228  
 229  
 230  
 231  
 232  
 233  
 234  
 235  
 236  
 237  
 238  
 239  
 240  
 241  
 242  
 243  
 244  
 245  
 246  
 247  
 248  
 249  
 250  
 251  
 252  
 253  
 254  
 255  
 256

### Figure captions

Fig. 1 – Rotational energy loss vs.  $J_p$  measured in a 0.640 mm thick low-carbon steel sheet in the range of frequencies 2 Hz - 1 kHz.

Fig. 2 – a) The experimental values of  $W_{\text{diff}}^{(\text{ROT})}(f) = W^{(\text{ROT})}(f) - W_{\text{class}}^{(\text{ROT})}(f)$  (symbols), with  $W_{\text{class}}^{(\text{ROT})}(f)$  given by Eq. (1), diverge from the standard  $f^{1/2}$  law beyond a threshold frequency, signaling the surge of the skin effect. b) At the same frequency the correspondingly calculated number of active magnetic objects  $n(H_{\text{exc}})$  versus  $H_{\text{exc}}$  behavior suffers a sharp turnabout.

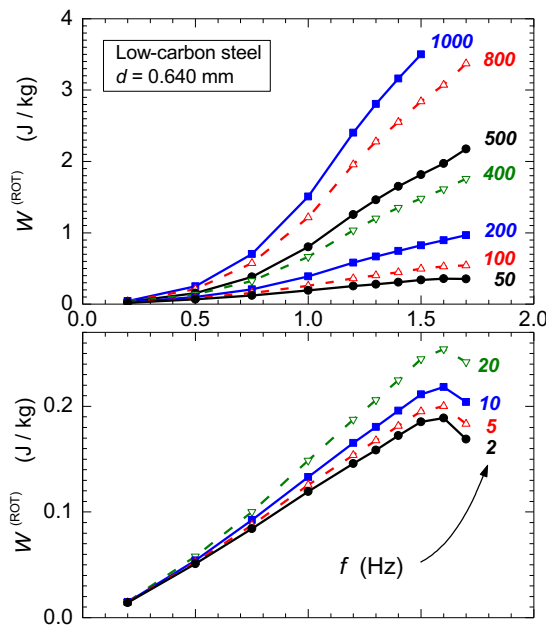
Fig. 3 – The experimental quasi-static  $H$ -locus is assimilated to a circular locus of same area, belonging to the equivalent perfectly isotropic material.

Fig. 4 – Quasi-static rotational permeability  $|\underline{\mu}| = B_p / H_0$  and related angular delay  $\square_{\text{hyst}}$  of  $B_p$  versus the rotating field  $H_0$

Fig. 5 – Skin effect dependent evolution of the hysteresis energy loss with frequency. Decrease of  $W_{\text{hyst}}^{(\text{ROT})}$  with  $f$  is observed at highest  $J_p$  values, because the material attains saturation on the outer sheet layers.

Fig. 6 – Measured rotational loss  $W_{\text{exp}}^{(\text{ROT})}$  versus polarization  $J_p$  at  $f=1$  kHz and  $f=100$  Hz and its comparison with the quantity  $W^{(\text{ROT,FP})} = W_{\text{hyst}}^{(\text{ROT})} + W_{\text{class}}^{(\text{ROT,FP})}$  (solid line) calculated via the electromagnetic diffusion equation and its solution by the Fixed Point technique. The dash-dotted lined shows the behavior of  $W_{\text{class}}^{(\text{ROT})}$  calculated with the standard Eq. (1).

Fig. 7 - Ratios  $F_{\text{class}}^{(\text{FP})} = W_{\text{class}}^{(\text{ROT,FP})} / W_{\text{class}}^{(\text{ROT})}$  and  $F_{\text{class}}^{(\text{LIN})} = W_{\text{class}}^{(\text{ROT,LIN})} / W_{\text{class}}^{(\text{ROT})}$  (with  $W_{\text{class}}^{(\text{ROT})}$  given by Eq. (1)) calculated by the numerical method with Fixed Point iteration and the linear method.  $d / \delta$  is the ratio between the sheet thickness and the skin depth.



257

258

259

260

261

262

263

Fig. 1 – Rotational energy loss versus circular polarization  $J_p$  measured in a 0.640 mm thick low-carbon steel sheet in the frequency range 2 Hz - 1 kHz.

264  
 265  
 266  
 267  
 268  
 269  
 270  
 271  
 272  
 273  
 274  
 275  
 276  
 277  
 278  
 279  
 280  
 281  
 282  
 283  
 284  
 285  
 286  
 287  
 288  
 289  
 290  
 291  
 292  
 293  
 294  
 295  
 296  
 297  
 298

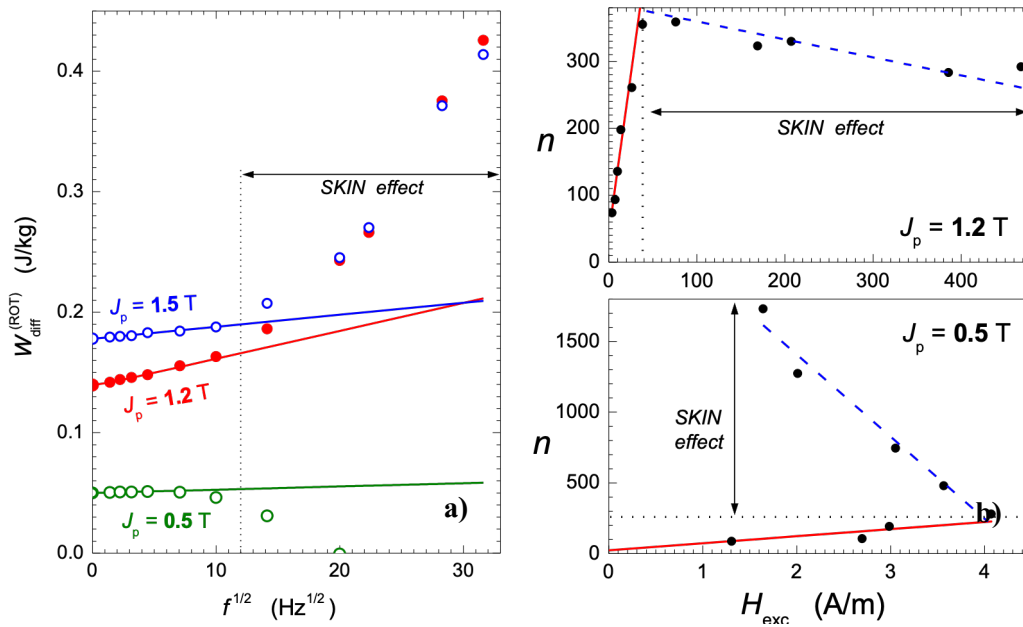
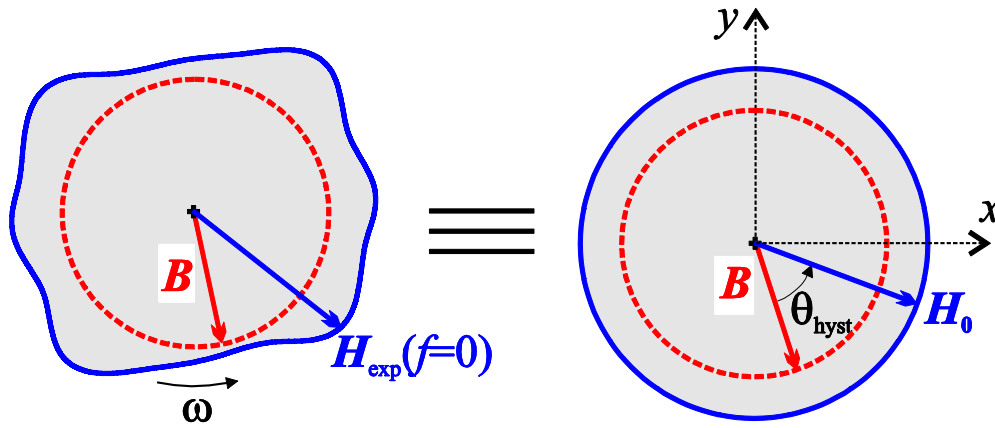


Fig. 2 – a) The experimental values of  $W_{\text{diff}}^{(\text{ROT})}(f) = W^{(\text{ROT})}(f) - W_{\text{class}}^{(\text{ROT})}(f)$  (symbols), with  $W_{\text{class}}^{(\text{ROT})}(f)$  given by Eq. (1), diverge from the standard  $f^{1/2}$  law beyond a threshold frequency, signaling the surge of the skin effect. b) At the same frequency the correspondingly calculated number of active magnetic objects  $n(H_{\text{exc}})$  versus  $H_{\text{exc}}$  behavior suffers a sharp turnabout.

299  
300  
301  
302  
303  
304  
305  
306

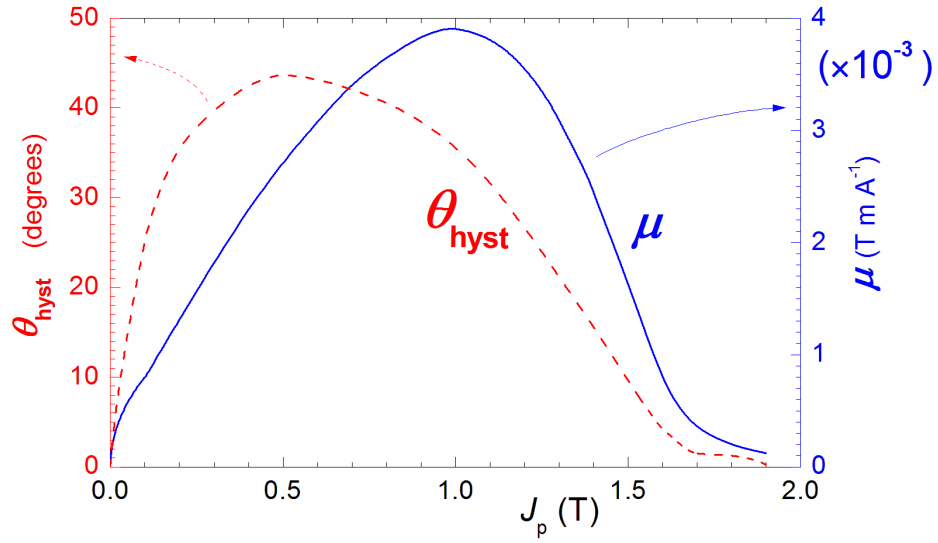


307  
308  
309

Fig. 1

Fig. 3 – The experimental quasi-static  $H$ -locus is assimilated to a circular locus of same area, belonging to the equivalent perfectly isotropic material.

310  
311  
312  
313  
314  
315  
316  
317  
318



319  
320  
321  
322  
323  
324  
325  
326  
327  
328  
329  
330  
331  
332  
333  
334  
335  
336  
337  
338  
339  
340

Fig. 4 – Quasi-static rotational permeability  $|\underline{\mu}| = B_p / H_0$  and related angular delay  $\theta_{\text{hyst}}$  of  $B_p$  versus the rotating field  $H_0$

341  
342  
343  
344  
345  
346  
347  
348  
349  
350  
351  
352  
353  
354  
355  
356  
357  
358  
359  
360  
361  
362  
363  
364  
365  
366  
367  
368  
369  
370  
371  
372  
373  
374  
375  
376  
377  
378  
379  
380  
381  
382  
383  
384  
385  
386  
387  
388  
389

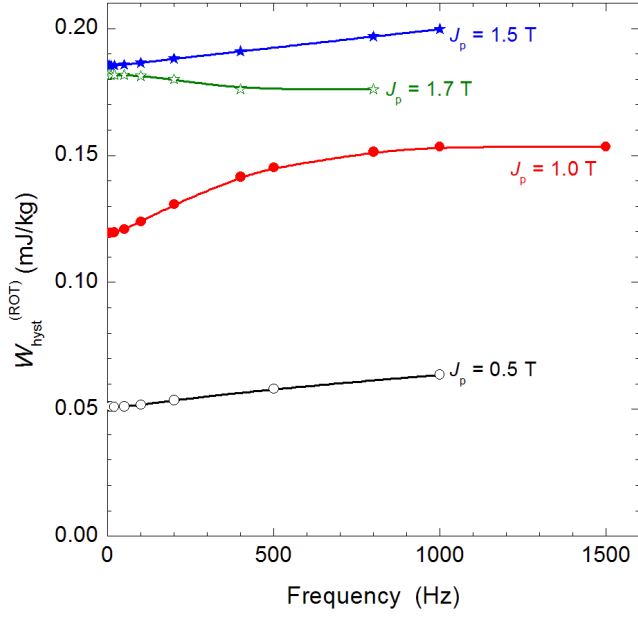


Fig. 5 – Skin effect dependent evolution of the hysteresis energy loss with frequency. Decrease of  $W_{\text{hyst}}^{(\text{ROT})}$  with  $f$  is observed at highest  $J_p$  values, because the material attains saturation in the outer sheet layers.

390  
 391  
 392  
 393  
 394  
 395  
 396  
 397  
 398  
 399  
 400  
 401  
 402  
 403  
 404  
 405  
 406  
 407  
 408  
 409  
 410  
 411  
 412  
 413  
 414  
 415  
 416  
 417  
 418  
 419  
 420  
 421  
 422  
 423  
 424  
 425  
 426  
 427  
 428  
 429  
 430  
 431  
 432  
 433  
 434  
 435  
 436  
 437  
 438  
 439

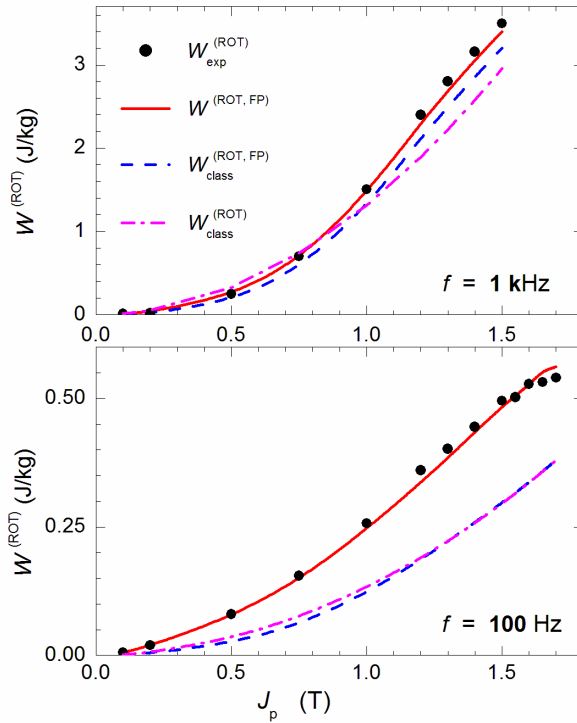


Fig. 6 – Measured rotational loss  $W_{exp}^{(ROT)}$  versus polarization  $J_p$  at  $f = 1 \text{ kHz}$  and  $f = 100 \text{ Hz}$  and its comparison with the quantity  $W^{(ROT, FP)} = W_{hyst}^{(ROT)} + W_{class}^{(ROT, FP)}$  (solid line) calculated via the electromagnetic diffusion equation and its solution by the Fixed Point technique. The dash-dotted lined shows the behavior of  $W_{class}^{(ROT)}$  calculated with the standard Eq. (1).



440  
 441  
 442  
 443  
 444  
 445  
 446  
 447  
 448  
 449  
 450

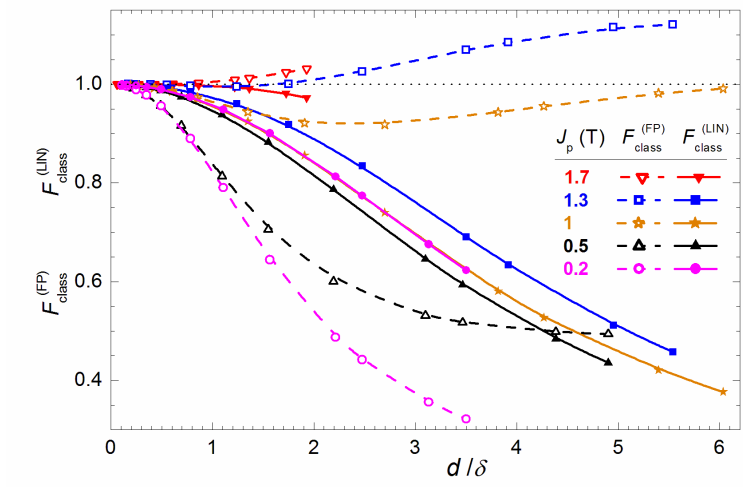


Fig. 7 - Ratios  $F_{class}^{(FP)} = W_{class}^{(ROT,FP)}/W_{class}^{(ROT)}$  and  $F_{class}^{(LIN)} = W_{class}^{(ROT,LIN)}/W_{class}^{(ROT)}$  (with  $W_{class}^{(ROT)}$  given by Eq. (1)) calculated by the numerical method with Fixed Point iteration and the linear method.  $d/\delta$  is the ratio between the sheet thickness and the skin depth.